Geoderma 468 (2026) 117780

Contents lists available at ScienceDirect

Geoderma

journal homepage: www.elsevier.com/locate/geoderma

Biogenic carbon input from *Spartina alterniflora* eradication governs nitrate removal pathways and N_2O emission in estuarine mangrove wetlands

Shiyao Chen [a,b,c], Hui Wu [a,b,c], Wenhong Xu [a,b,c], Fenfang Wang [d], Ruifeng Yan [e], Shaobin Li [a], Nengwang Chen [a,b,c,*]

[a] Fujian Provincial Key Laboratory for Coastal Ecology and Environmental Studies, College of the Environment and Ecology, Xiamen University, Xiamen 361102, China
[b] State Key Laboratory of Marine Environment Science, Xiamen University, Xiamen 361102, China
[c] National Observation and Research Station for the Taiwan Strait Marine Ecosystem, Xiamen University, Zhangzhou 363300, China
[d] Polar and Marine Research Institute, College of Harbor and Coastal Engineering, Jimei University, Xiamen 361021, China
[e] State Key Laboratory of Urban Water Resource and Environment, School of Environment, Harbin Institute of Technology, Harbin 150090, China

ARTICLE INFO

Handling Editor: Dr Diego Abalos

Keywords:
Spartina alterniflora eradication
Coastal wetland
Ecological restoration
Nitrous oxide
Denitrification

ABSTRACT

Estuarine mangrove wetlands mitigate coastal eutrophication by removing nitrate (NO_3^-); however, the effects of invasive *Spartina alterniflora* eradication, a key biogenic carbon source, on NO_3^- removal pathways and nitrous oxide (N_2O) emissions remain poorly understood. Here, we conducted a two-year field observation and laboratory anaerobic sediment incubation amended with plant residues, combined with ^{15}N isotope tracing and metagenomics analyses. Field observation and laboratory incubation experiments revealed that during the initial eradication, the elevated organic carbon from *Spartina alterniflora* degradation stimulated denitrifying bacteria (e.g., *Proteobacteria*) and the *nirS* gene abundance. Consequently, NO_3^- removal was dominated by denitrification (DNF, 90.26%), while dissimilatory nitrate reduction to ammonium (DNRA) contributed minimally. Meanwhile, the concurrent pH decline from plant residue fermentation inhibited *nosZ*-mediated reduction, leading to incomplete DNF and a consequent 153.0% rise in N_2O emissions above the background level of 12.48 μg m^{-2} h^{-1}. The DNF contribution and N_2O emission increase reached their maximum approximately six months after plant removal. Driven by an elevated C: NO_3^- ratio from continuous organic carbon accumulation and NO_3^- consumption over the following two years, DNRA contribution rose from 5.78% to 34.34% alongside a shift of N_2O flux to a sink (−14.54 μg m^{-2} h^{-1}). The accumulation of *nrfA* gene, sulfate-reducing bacteria, and II type *nosZ* microorganisms (e.g., *Bacteroidetes, Thermodesulfobacteria*) in the sediments favored the above conversion. This study elucidates how biogenic carbon addition reconfigures NO_3^- removal pathways and associated ecosystem functions, providing scientific insights for coordinating ecosystem management restoration with climate change goals.

1. Introduction

Estuarine mangrove wetlands are critical transitional zones between land and ocean, serving as hotspots for nutrient transformation and removal (Chiu et al., 2004; McCall and Pennings 2012). Nitrate (NO_3^-) plays a pivotal role as the dominant form of reactive nitrogen (Jia et al., 2016), with its fate determined by the competition between denitrification (DNF) and dissimilatory nitrate reduction to ammonium (DNRA) (Beaulieu et al., 2011; Zheng et al., 2016). While DNF is responsible for 87–89% of nitrogen removal in mangrove sediments (Wang and Lin 2023), it can also be a major source of N_2O emissions due to incomplete DNF, a 100-year global warming potential 273 times greater than CO_2 (Beaulieu et al., 2011; IPCC 2021). Conversely, DNRA retains NO_3^- as bioavailable NH_4^+ and does not produce N_2O (Fan et al., 2024). This inherent trade-off between nitrogen removal via DNF and its climate impact underscores that the partitioning of NO_3^- removal pathways is fundamental to predicting N_2O emissions.

The invasion of *Spartina alterniflora* (*S. alterniflora*) is widely

* Corresponding author at: Fujian Provincial Key Laboratory for Coastal Ecology and Environmental Studies, College of the Environment and Ecology, Xiamen University, Xiamen 361102, China.
E-mail addresses: shiyaochen@stu.xmu.edu.cn (S. Chen), wuhui@stu.xmu.edu.cn (H. Wu), 33120221152251@stu.xmu.edu.cn (W. Xu), ffwang@jmu.edu.cn (F. Wang), 24b329014@stu.hit.edu.cn (R. Yan), shaobinli@xmu.edu.cn (S. Li), nwchen@xmu.edu.cn (N. Chen).

https://doi.org/10.1016/j.geoderma.2026.117780
Received 28 October 2025; Received in revised form 4 March 2026; Accepted 13 March 2026
Available online 17 March 2026
0016-7061/© 2026 The Author(s). Published by Elsevier B.V. This is an open access article under the CC BY license (http://creativecommons.org/licenses/by/4.0/).

recognized as a major and widespread ecological threat to coastal wetlands across China (Chen et al., 2022). Previous studies report that *S. alterniflora* invasion in mudflats enhances DNF and increases N_2O emissions, largely due to elevated organic carbon (OC) inputs (Gao et al., 2019; Yuan et al., 2015). To restore wetland ecological functions and biodiversity, China has initiated the world's largest coastal wetland restoration program, aiming to eradicate over 90% of *S. alterniflora* in each coastal province by 2025 (Stokstad 2023; Zhu et al., 2024). The eradication of *S. alterniflora* is primarily carried out through mowing and plowing, processes that introduce large amounts of plant residues into the sediments (Tang et al., 2021). In contrast to the gradual carbon enrichment caused by invasion, eradication delivers a concentrated pulse of residue-derived organic matter characterized by relatively high C/N ratios (Lu et al., 2023) and slower decomposition rates (Lee et al., 2026; O'Nuanain et al., 2025). Such a substantial pulse of biogenic carbon can significantly reshape sediment redox gradients, alter substrate stoichiometry, and restructure microbial communities (Crow et al., 2009; Kuzyakova et al., 2000; Wang et al., 2023b). However, how these alterations in sediment conditions affect NO_3^- removal pathways and associated N_2O emissions remains unclear.

The balance between DNF and DNRA is known to be highly sensitive to environmental factors such as NO_3^- concentration, organic carbon availability, C/ NO_3^- ratios, and redox-sensitive electron donors (Fan et al., 2024; Fazzolari et al., 1998; Liao et al., 2025; Shao et al., 2025). Moderate carbon enrichment tends to enhance DNF by providing readily available electron donors (Lopez-Ponnada et al., 2017), whereas excessive or recalcitrant carbon, particularly under NO_3^- limited conditions, often shifts NO_3^- reduction toward DNRA (Sun et al., 2021; Wei et al., 2022). Meanwhile, the anaerobic decomposition of *S. alterniflora* residues promotes sulfate reduction and the accumulation of sulfide (Wang et al., 2019a), which serves as an alternative electron donor for both DNRA and chemolithotrophic DNF (Aelion and Warttinger 2010; Burgin and Hamilton 2007; Song et al., 2016). These intertwined carbon–sulfur–nitrogen interactions suggest that eradication induced carbon inputs may reconfigure NO_3^- removal pathways through altered microbial competition for electron donors.

NO_3^- reduction pathways also have important implications for N_2O dynamics (Jia et al., 2016; Zheng et al., 2016). Previous studies suggest that plant residue incorporation often stimulates N_2O production by supplying labile organic carbon and nitrogen, which stimulates DNF activity (Surey et al., 2020; Wang et al., 2023b). In addition, fermentation-derived low-molecular-weight organic acids (e.g., acetate, lactate) can inhibit N_2O reductase activity, leading to greater N_2O accumulation (Su et al., 2021; Zhu et al., 2022). However, the decomposition of recalcitrant residues may suppress microbial extracellular enzyme activity, thereby limiting the availability of labile carbon for denitrifiers (Feng et al., 2024; Wang et al., 2019b). Furthermore, when inorganic nitrogen is scarce or carbon substrates are chemically complex, the priming effect on N_2O emissions may be attenuated (Tao et al., 2022; Xu et al., 2023). These opposing mechanisms highlight the complexity of biogeochemical responses following *S. alterniflora* eradiation.

Despite the ecological importance of these processes, a critical knowledge gap remains: it is unclear how eradication-induced biogenic carbon inputs modify NO_3^- removal pathways and regulate N_2O emissions in estuarine mangrove wetlands. To address this gap, we aimed to elucidate how varying amounts of *S. alterniflora* residues influence the fate of NO_3^- and the associated N_2O emissions following eradication. In this study, we combined field monitoring, laboratory incubations, isotopic tracing, and metagenomic analyses to disentangle the biogeochemical and microbial mechanisms underlying these processes. This study provides a mechanistic framework for understanding how *S. alterniflora* eradication reshapes nitrogen transformation pathways and offers insights for optimizing wetland restoration strategies to enhance nutrient removal efficiency while mitigating greenhouse gas emissions.

2. Materials and methods

2.1. Study area and field observation

Sampling sites were located in Zhangjiang Estuary Mangrove National Nature Reserve, Zhangzhou, Fujian Province, China (Fig. 1), with coordinates of 117°24′–117°30′E and 23°53′–23°56′N. The mangrove wetland has a semidiurnal tidal pattern, with an average tidal range of 2.32 m (Zhu et al., 2019). The study area has a subtropical monsoon climate, with an annual mean temperature of 22.8 ± 5.7 °C and annual precipitation of 1679 mm, while monthly rainfall ranged from 1 to 404 mm (Wang et al., 2022). Similar to many intertidal wetlands, *S. alterniflora* has rapidly expanded in this wetland over the past decades, transforming the landscape from a bare mudflat to a vegetated habitat. In late October 2022, the government implemented a large-scale excavation-based removal of *S. alterniflora*, restoring the wetland to a mudflat-dominated state within two weeks (Zhu et al., 2024).

To investigate field N_2O flux dynamics at the sediment-air interface in post-eradication *S. alterniflora* habitats, we conducted three field observations in April 2023, November 2023, and October 2024. Adjacent mudflats were simultaneously monitored and sampled for comparative analysis (Fig. 1a). The procedures for N_2O collection and quantification are described in Text S1.

For physicochemical analysis and incubation experiments, sediment samples (0–40 cm depth) were collected in triplicate during low tide from two sites (an *S. alterniflora* eradication area and a mudflat; Fig. 1a) using plexiglass corers (Φ 120 mm × 500 mm). The three cores from each site were then combined to form a single composite sample for analysis. The samples were then homogenized and stored in an anaerobic cryogenic freezer. Upon arrival at the laboratory, the sediment was thoroughly stirred and passed through a 20-mesh sieve to remove plant residues and stones. Meanwhile, in-situ seawater was collected from a nearby tidal creek using collapsible sampling bags and subsequently filtered through 0.7 μm glass-fiber filters (GF/F Whatman).

2.2. Sediment incubation experiment

Considering that the aboveground biomass of *S. alterniflora* in our region ranges from 0.24 to 3.69 kg dry m^{-2} (Huang et al., 2023), three levels of detritus addition (0, 2, and 4 kg dry m^{-2}) were established to simulate different eradication intensities, defining as no addition (CK, 0 kg m^{-2}), low addition (L, 2 kg m^{-2}), and high addition (H, 4 kg m^{-2}) to simulate no eradication, low-intensity eradication, and high-intensity eradication. Based on the sediment bulk density of 0.8 g cm^{-3} and the plowing depth of 0.4 m, these levels corresponded to the addition of 0, 0.075, 0.15 g of *S. alterniflora* dry residues to approximately 60 g of slurry (equivalent to 10 g dry sediment). Whole plants of *S. alterniflora* were oven-dried at 65 °C, cut into fragments, and finely ground using a ball mill homogenizer (JXFSTPRP, Jingxin, China). The detritus was added three days prior to the start of incubation (before aeration). Sediment slurries were prepared by mixing sediments with in-situ seawater (n = 3; Table S1), which had been filtered through 0.7 μm glass-fiber filters (Whatman GF/F, USA). The bottles were purged with high-purity He at a flow rate of 60 mL min^{-1} for at least ten gas exchange cycles to remove dissolved O_2 and establish anaerobic conditions (Chen et al., 2023). Thereafter, the microcosms were incubated in the dark at the in-situ temperature (25 °C) in a constant-temperature chamber.

Overlying water and sediment samples were collected in triplicate on day 0, 0.5, 1, 3, 5, 7, 14, and 21 for physicochemical analyses, as well as for measurements of N_2O and N_2 production. The sediment samples were assessed for water content (WC), total organic carbon (TOC), total nitrogen (TN), total sulfur (TS), ammonia nitrogen (NH_4^+), and NO_3^-. The overlying water was analyzed for concentrations of NH_4^+, NO_3^-, nitrite (NO_2^-), dissolved inorganic carbon (DIC), dissolved organic carbon (DOC), and sulfate (SO_4^{2-}). For nitrogen transformation incubations, sediment slurries were prepared at a 1:5 sediment-to-seawater ratio on

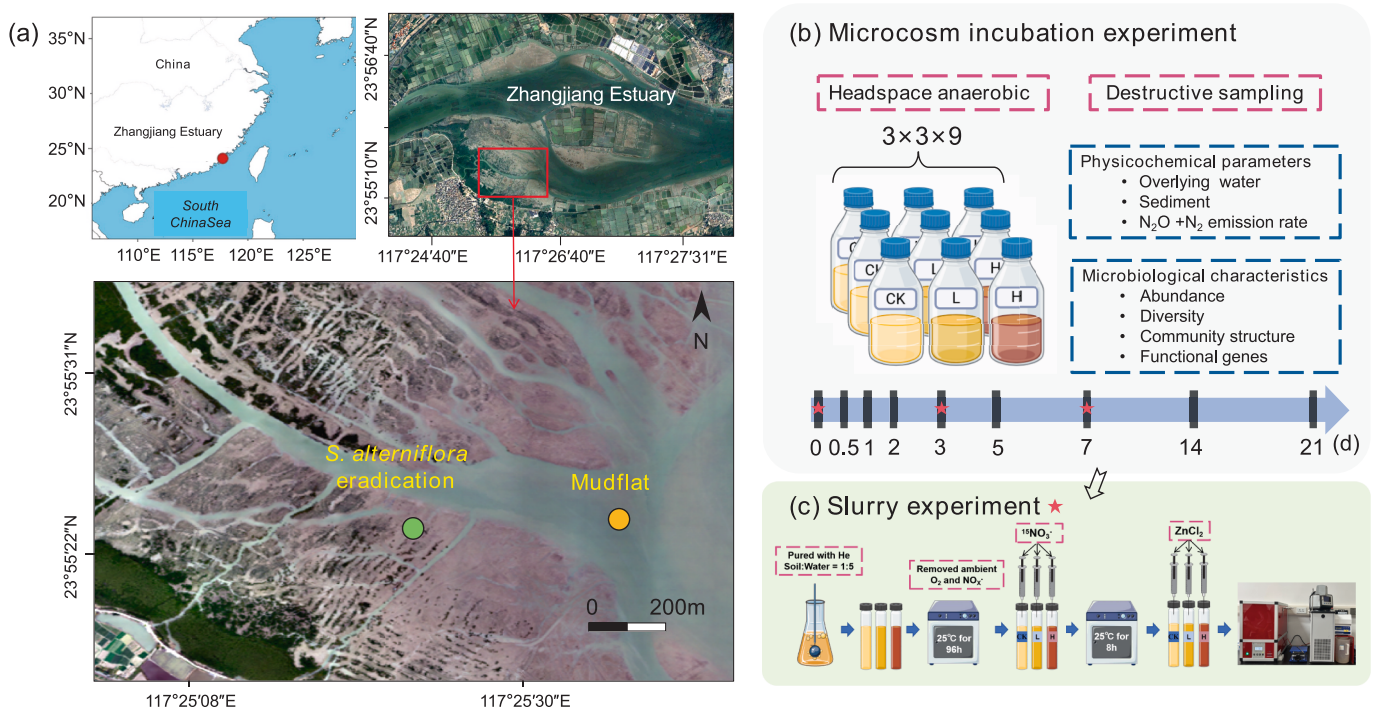


Fig. 1. Sampling sites and experiment design of this study. (a) Study area and sampling sites. are indicated by green and orange circles, representing the *S. alterniflora* eradication habitat and the mudflat habitat, respectively. (b) Illustration of microcosm incubation experiments. (c) Illustration of slurry incubation experiments.

day 0, 3, and 7. Potential rates of DNF, ANA, and DNRA were determined using the ^{15}N isotope-pairing technique (Hou et al., 2014; Wang et al., 2023a) with $^{15}NO_3^-$ amendments under anaerobic conditions (Fig. 1c). Detailed calculation procedures are provided in the Supplementary Methods (Text S2).

2.3. Physicochemical properties measurements

Sediment WC was calculated gravimetrically from fresh sediment freeze-dried to a constant value. The pH of the sediment was measured using a WTW multiparameter meter (Multi 3430, Germany). After rinsing with 1 M hydrochloric acid and passing through the 100-well mesh sieve, ground samples were used to determine TOC and TN using a CHNS elemental analyzer (Elementar Vario EL cube, Germany) (Wang et al., 2023a). The concentrations of NH_4^+ and NO_3^- were determined for both sediment extracts (with 1 M KCl) and overlying water using a continuous flow nutrient analyzer (AA3, SEAL Analytical, Germany). The concentrations of dissolved N_2O were determined using a headspace equilibration technique and a gas chromatograph (Agilent 7890A, US). Dissolved N_2 concentrations were measured using the N_2: Ar method in a membrane inlet mass spectrometer (Chen et al., 2010). Details about the calculation of excess production of N_2 (ΔN_2) and N_2O production are shown in the supporting information (Text S3 and S4). DIC concentration was determined by CO_2/H_2O analyzer (LI 7000). DOC of overlying water was determined with a Shimadzu TOC-TN analyzer (Shimadzu, Japan) (Lu et al., 2023). Quantitative analysis of water-soluble ion SO_4^{2-} was performed using an ion chromatograph (Thermo ICS-1100).

2.4. DNA sequencing and metagenomic sequencing

DNA was extracted from 0.5 g of wet sediment using the HiPure Soil DNA Kit B (Magen, China). DNA quality was assessed by a NanoDrop (Thermo Scientific, USA), and concentration was measured using a Qubit 4 Fluorometer (Thermo Scientific, USA). Each sample was then amplified by PCR for 8 cycles using P5 and P7 primers, and the PCR products were cleaned up and validated using an Agilent 2100 Bioanalyzer. The qualified libraries were sequenced paired-end PE150 on the Illumina HiSeq platform.

Raw sequences were processed with bcl2fastg (v2.17.1.14) for base calling and converted to FASTQ. Adaptors and low-quality reads were removed with cutadapt (v1.9.1). Clean reads were assembled using MEGAHT (v1.1.3) (Martin 2011), and coding sequences were predicted with Prodigal (v3.02) (Hyatt et al., 2010). A non-redundant unigene set was generated using MMseq2 (95% sequence identity and 95% coverage thresholds) (Steinegger and Söding 2017). Gene abundance was calculated by mapping clean reads to unigene sequences with Soap Aligner (v2.21) (Li et al., 2009). Predicted proteins were annotated against the KEGG Genes and NCBI NR databases using DIAMOND (v0.8.15.77) (Buchfink et al., 2015) with an e-value cut off of 1e-5 and minimum identity of 30%.

2.5. Statistical analyses

Values are expressed as mean ± standard deviation based on three parallel samples (n = 3) for each treatment or observation time. Prior to parametric testing, data were examined for normality (Shapiro-Wilk test) and homogeneity of variance (Levene's test). Statistical analyses of environmental parameters, N_2O production, and nitrogen transformation rates were conducted in R 4.3.2, with differences among treatments tested using one-way ANOVA and Tukey's HSD post-hoc comparison ($p < 0.05$). Note that the units in this study are all transformed to sediment dry weight unless otherwise noted.

The α-diversity analysis was based on the species-level results, and the Bray-Curtis distance of bacterial composition was calculated by the "vegan" package and non-metric multi-dimensional (NMDS). Spearman correlations were applied to assess pairwise associations between environmental variables and nitrogen transformation processes. Mantel tests were performed using Bray-Curtis distance matrices to evaluate correlations between environmental variables and functional microbial communities at the genus level. Redundancy analysis (RDA) was conducted to explore the relationships between environmental variables

and the combined phylum-level community and functional gene composition matrix. To investigate the interaction between microbial community and functional genes, microbial co-occurrence networks were constructed using the ggClusterNet package (Wen et al., 2022) based on samples from the ambient control and the *S. alterniflora* treatments and visualized using Gephi (v0.9.2).

3. Results

3.1. Field N_2O emissions and incubation N_2O production rates

Significant differences in field N_2O emission fluxes were observed before and after the eradication of *S. alterniflora* (Fig. 2a). Field monitoring six months post-eradication (April 2023) showed that flux reached 31.60 ± 2.33 μg m^{-2} h^{-1}, representing a 153% increase over the natural *S. alterniflora* sediment flux of 12.48 μg m^{-2} h^{-1} ($p < 0.01$) (Gao et al., 2019). As eradication continued, N_2O emission fluxes declined significantly ($p < 0.01$). After one to two years of eradication, N_2O fluxes in *S. alterniflora* habitats decreased to −9.96 ± 2.14 and −27.93 ± 0.76 μg m^{-2} h^{-1}, respectively. This constituted a net change of −41.56 and −59.53 μg m^{-2} h^{-1}, effectively reversing the habitat from a strong N_2O source to a net sink.

Laboratory incubations showed that *S. alterniflora* residues addition and incubation time significantly influenced N_2O production. Rates peaked on day 1 at 14.66 ± 0.80 and 50.25 ± 0.71 μg kg^{-1} h^{-1} in the low and high addition treatments, respectively, significantly higher than the no addition treatment (2.22 ± 0.04 μg kg^{-1} h^{-1}; $p < 0.01$). Rates dropped sharply by day 3 and stabilized near background levels. The $N_2O/(N_2O + N_2)$ ratio mirrored this trend, highest in high addition treatment on day 1 (0.19 ± 0.02%) but declining sharply thereafter as N_2 became the dominant gas.

3.2. Change in overlying water and sediment properties of the incubation experiment

The incubation experiment demonstrated that incorporating *S. alterniflora* residues significantly altered the physicochemical properties of both sediment and overlying water in a dose-dependent manner (Fig. 3 & Fig. S1). In sediments, residue additions led to a significant increase in WC, TOC, NH_4^+, and TS, while NO_3^- decreased markedly. Specifically, the high addition treatment exhibited a 25.08% increase in TOC and a 67.50% surge in NH_4^+ compared to the no addition treatment. Sediment pH did not change significantly over time but differed markedly among treatments ($p < 0.01$), decreasing with the residue addition level: 7.83 ± 0.03 in no addition, 7.73 ± 0.05 in low addition, and 7.59 ± 0.09 in high addition (Fig. S2b). Field sediment properties showed consistent patterns, with slightly lower pH and elevated TOC and DOC in eradicated plots (Table 1), confirming that incubation trends reflect natural conditions.

Overlying water pH dropped sharply in the initial 24 h, with decreases of 9.40% in low addition and 12.54% in high addition, compared to only 1.95% in the no addition tretment treatment (Fig. S1a; $p < 0.01$). The decrease in NO_3^- concentration in different treatment groups showed significant differences. The concentrations in the low and high additions decreased by 94.36% and 97.63% within 3 days, respectively, while that in the no addition treatment only decreased by 34.25%. DOC increased sharply on day 1, with the high addition reaching a concentration 8.78 times that of no addition, followed by a subsequent decline. The decrease in SO_4^{2-} after day 3 coincided with a rise in DIC.

3.3. Change in sediment NO_3^- reduction rates

The DNF rates at the initial cultivation stage demonstrated a marked increase in both the low addition (24.40 ± 0.65 μmol h^{-1} kg^{-1}) and high addition (21.43 ± 3.19 μmol h^{-1} kg^{-1}) compared to the no addition (11.54 ± 1.08 μmol h^{-1} kg^{-1}) ($p < 0.05$; Fig. 4a). The DNF rate in the high addition was 12.2% lower than that in the low addition, indicating a non-dose-dependent relationship between the addition of *S. alterniflora* and the DNF rate. As cultivation progressed, the DNF rates in all treatment groups exhibited a pronounced reduction relative to day 0 ($p < 0.01$).

The DNRA rates exhibited distinct temporal dynamics across treatment groups (Fig. 4b). During the 7-day incubation, the rates in the no addition treatment remained low and stable, increasing only 1.12-fold (from 0.15 ± 0.01 to 1.16 ± 0.16 μmol h^{-1} kg^{-1}). In contrast, the groups, low and high addition showed marked, dose-dependent increases, rising 2.25-fold (from 0.22 ± 0.15 to 2.23 ± 1.10 μmol h^{-1} kg^{-1}) and 3.61-fold (from 1.80 ± 0.11 to 6.50 ± 1.15 μmol h^{-1} kg^{-1}), respectively. These increases were both significantly greater than those in the no addition treatment ($p < 0.01$).

The addition of *S. alterniflora* residues significantly shifted the partitioning of NO_3^-reduction ($p < 0.05$; Fig. 4c). Specifically, the contribution of DNRA increased from 0.85% to 18.09% in the low addition and from 7.25% to 44.57% in the high addition. Conversely, the dominance of DNF declined from 92.28% to 74.60% and from 86.47% to 49.07% in the low and high addition, respectively. Overall, at the end of

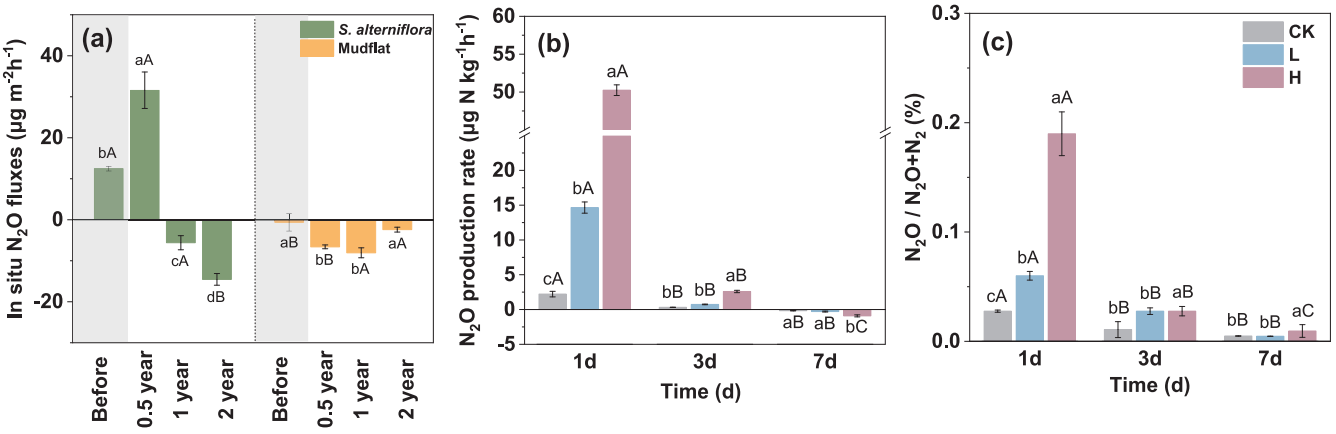


Fig. 2. Changes of in-situ N_2O fluxes in *S. alterniflora* and mudflat zones during the pre- and post-eradication periods (a), potential N_2O production rates (b), and $N_2O/(N_2O + N_2)$ ratios (c) under different *S. alterniflora* residue additions. Error bars represent standard deviation (n = 3). CK, L, and H denote control (no eradication, 0 kg m^{-2}), low-intensity eradication (2 kg m^{-2}), and high-intensity eradication (4 kg m^{-2}), respectively. The gray and white backgrounds denote pre- and post-eradication periods, respectively. Data in pre-eradication periods are from refs (Gao et al., 2019). Monitoring time points included 0.5 years (April 2023), 1 year (November 2023), and 2 years (October 2024) after eradication. Different lowercase letters indicate significant differences among the treatments ($p < 0.05$), and the uppercase letters denote significant differences ($p < 0.05$) on different days at the *S. alterniflora* residue additions.

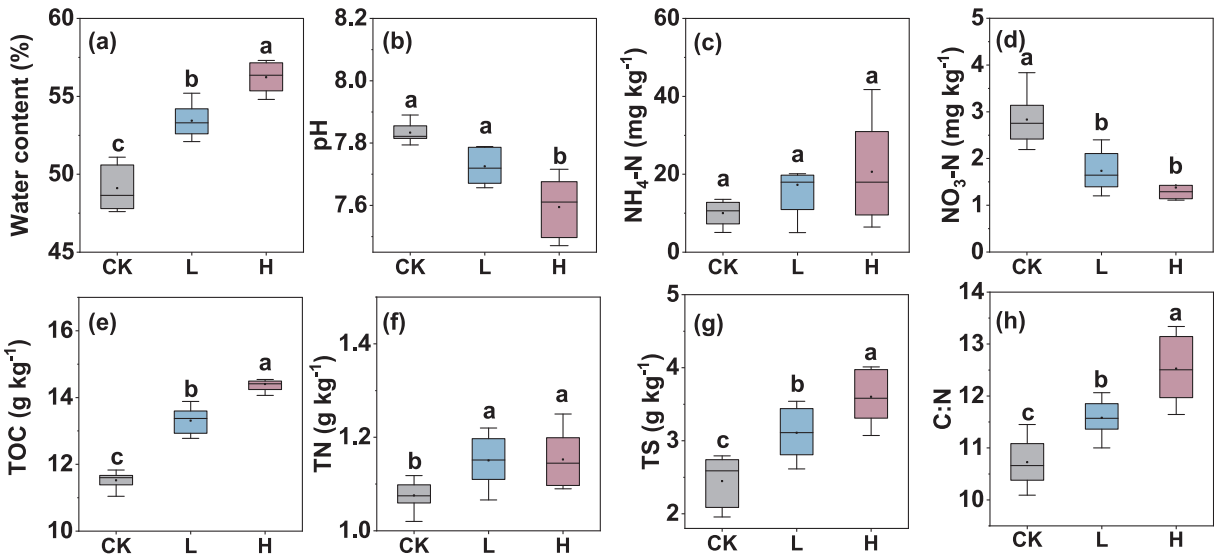


Fig. 3. Physicochemical properties of sediment under different *S. alterniflora* residue additions. CK, L, and H denote control (no eradication, 0 kg m^{-2}), low-intensity eradication (2 kg m^{-2}), and high-intensity eradication (4 kg m^{-2}), respectively. Boxplots display variation between time points, and different lowercase letters indicate significant differences among the treatments ($p < 0.05$). Error bars represent standard deviation (n = 3).

Table 1
Comparison of physical and chemical parameters of sediments before and after *S. alterniflora* eradication compared with mudflat in field observation.

Time	Before	0.5 year	1 year	2 year	Mudflat
Water Content (%)	41.59^{b}	49.83^{a}	47.92^{a}	48.05^{a}	40.59^{b}
Eh (mV)	-46.22^{a}	-16.58^{b}	-34.47^{b}	-45.63^{a}	-24.42^{b}
pH	7.78^{a}	7.17^{b}	7.47^{a}	7.66^{a}	7.40^{a}
NH_4^+-N (mg kg^{-1})	13.58^{b}	5.14^{b}	42.21^{a}	37.38^{a}	5.98^{b}
NO_3^--N (mg kg^{-1})	0.95^{a}	0.68^{b}	0.59^{b}	0.81^{a}	1.01^{a}
DOC (mg kg^{-1})	NA	17.73^{ab}	33.55^{a}	30.35^{b}	4.72^{b}
TOC (g kg^{-1})	10.05^{a}	11.86^{a}	10.36^{a}	12.35^{a}	7.79^{b}
TN (g kg^{-1})	1.08^{a}	1.20^{a}	0.99^{a}	1.15^{a}	0.56^{b}
TS (g kg^{-1})	NA	2.83^{b}	3.63^{a}	3.92^{a}	2.05^{b}
TOC:TN	9.73^{a}	9.88^{b}	10.46^{b}	10.74^{b}	13.91^{a}
TOC:NO_3^-	10.57^{b}	13.79^{a}	17.56^{a}	15.25^{a}	7.71^{b}
DOC:NO_3^-	NA	26.07^{a}	33.89^{a}	37.47^{a}	3.01^{b}
DNF Rate (μmol $h^{-1}kg^{-1}$)	15.70^{ab}	28.90^{a}	6.16^{b}	7.88^{b}	3.14^{b}
DNRA Rate (μmol $h^{-1}kg^{-1}$)	1.28^{b}	1.85^{b}	2.79^{ab}	4.78^{a}	1.98^{b}
ANA Rate (μmol $h^{-1}kg^{-1}$)	1.55^{a}	1.27^{a}	0.92^{a}	1.26^{a}	0.62^{a}

Data characterizing the pre-eradication status of *S. alterniflora* were obtain from (Wang and Lin 2023) and (Wang et al., 2023). The affiliated letters a and b indicate significant differences among sediments before and after *S. alterniflora* eradication compared with mudflat reaches at the 95% confidence level. NA means no data available.

the incubation, DNRA% in the low and high addition represented 1.13-fold and 2.79-fold increases, respectively, compared to the control.

The ANA rates remained low and relatively stable across all incubation stages (from 0.77 ± 0.06 to 2.10 ± 0.21 μmol h^{-1} kg^{-1}; $p > 0.05$), contributing only 6.28–15.62% of total NO_3^- transformations (Fig. S4). This indicates that ANA was a minor pathway compared to DNRA and DNF under the addition of *S. alterniflora* residues.

3.4. Microbial community structure and functional gene profile

The addition of *S. alterniflora* residues significantly altered the sediment microbial community structure and enhanced its species richness, as indicated by a significant increase in ACE and Chao1 indices in the low and high addition compared to the no addition treatment (Table S2, $p < 0.05$). This structural shift was confirmed by Bray-Curtis-based NMDS and ANOSIM analyses, which revealed clear separation between the no addition treatment and residue-amended treatments ($R^2 = 0.68$, $p = 0.008$).

The top five dominant phyla across treatments were *Proteobacteria, Bacteroidota, Thermodesulfobacteriota, Myxococota*, and *Clostridium* at the phylum level. While *Proteobacteria* had the highest relative abundance in all treatments, its abundance in the high addition initially (60.30 ± 0.75%) was higher than in no addition (54.16 ± 0.63%) and low addition (53.35 ± 1.31%), but dropped to 34.85 ± 0.23% by day 7, significantly lower than in no addition (46.97 ± 0.31%) and low addition (39.77 ± 1.11%) ($p < 0.05$). *S. alterniflora* residue additions also significantly increased the abundance of *Bacteroidota*, *Thermodesulfobacteriota*, and *Bacillus* ($p < 0.05$). The addition of *S. alterniflora* residues resulted in a decrease in DNF-associated genera (*Pseudomonas, Gemmatimonas*) while significantly increasing the abundance of DNRA-associated genera (*Clostridium, Shewanella, Vibrio*) (Fig. 6). The co-occurrence network analysis revealed that *S. alterniflora* treatments decreased the number of links, graph density, modules, and modularity but increased the percentage of positive links, compared to the control (Table S5).

The addition of *S. alterniflora* significantly reshaped the functional gene profiles related to nitrogen, sulfur cycling, and carbon degradation (Fig. 5c). Consistent with the potential DNF rate trend in the early reaction stage, it significantly upregulated the relative abundance of DNF-related functional genes *nirS* ($p < 0.05$). However, the *nosZ* gene relative abundance in the high addition was significantly lower than in the control and low additions initially (Fig. 5c). The relative abundance of genes related to DNRA (*nrfA*) was significantly higher in the high addition. After the addition of *S. alterniflora*, the relative abundance of carbon degradation-related functional genes showed a systematic increase: the relative abundance of starch degradation genes (*amyA/B*) and cellulose degradation genes (*celB, xynA/B*) increased with incubation time (Fig. 5d), indicating the gradual breakdown of lignocellulosic materials. And sulfate reduction-related functional genes (*aprA, aprB, sat, sqr*) generally increased (Fig. 5e), with *sat* and *aprA* showing the most significant increases. Additionally, the relative abundance of C degradation-related genes increased at all sites, and the enrichment of fermentation genes (*acsA* and *mcrA*) and the synchronous upregulation of *bamB* suggest that the generation of metabolites like acetate and H_2 may further drive the sulfur cycle.

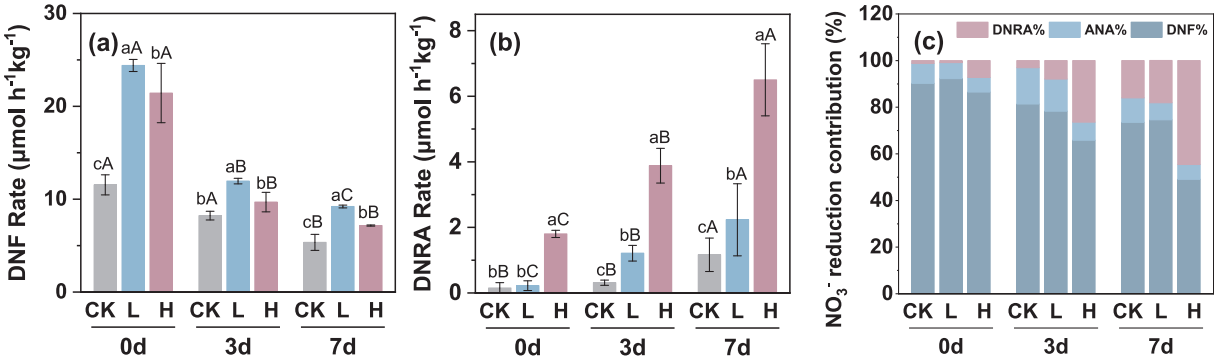


Fig. 4. Temporal dynamics of (a) potential DNF rates, (b) DNRA rates, (c) the relative contribution of NO_3^- reduction pathways. CK, L, and H denote control (no eradication, 0 kg m^{-2}), low-intensity eradication (2 kg m^{-2}), and high-intensity eradication (4 kg m^{-2}), respectively. DNRA% represents the proportion of DNRA to total nitrate reduction, calculated as DNRA/(DNF + DNRA). Error bars represent standard deviations (n = 3). Different lowercase letters indicate significant differences ($p < 0.05$) among addition levels on the same day; different uppercase letters indicate significant differences ($p < 0.05$) among days for the same addition level.

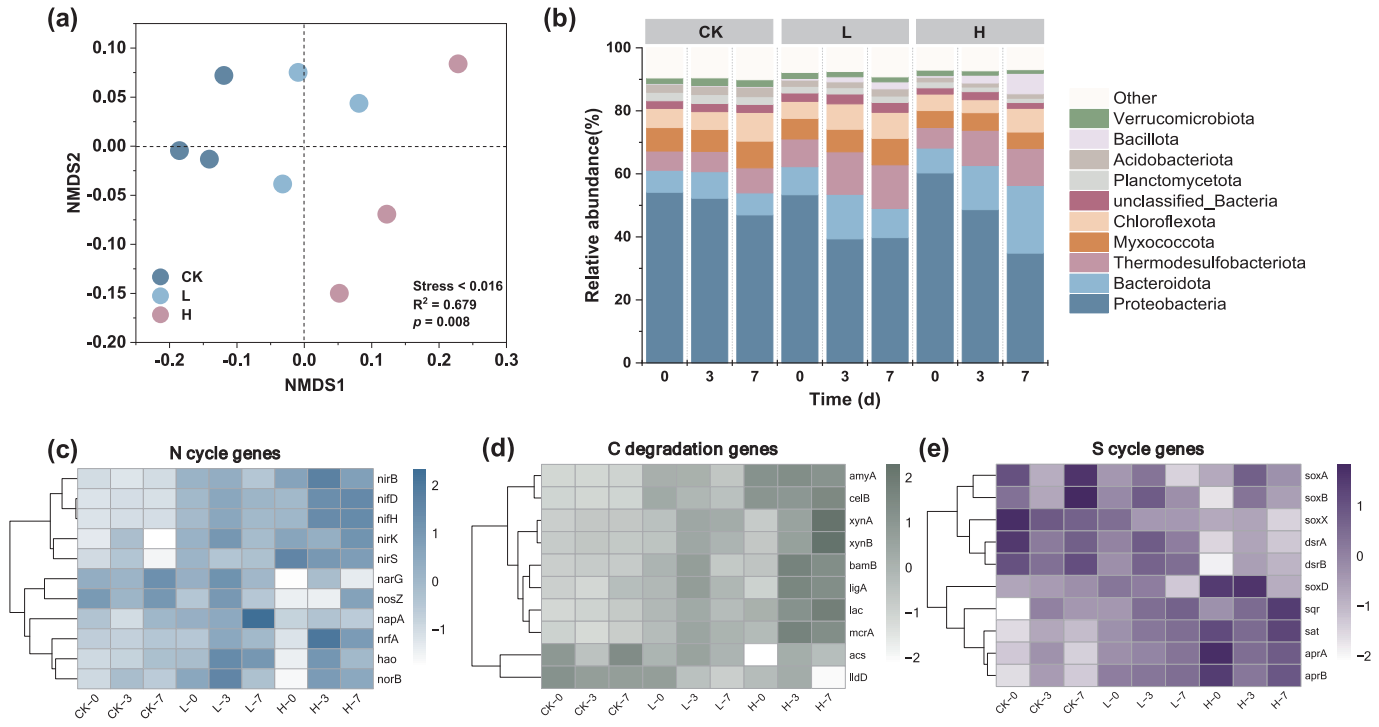


Fig. 5. The effect of *S. alterniflora* residue additions on the structure of microbial communities and genes in sediments. (a) Non-metric multi-dimensional (NMDS) based on Bray-Curtis distance of microbial communities. (b) Microbial classification at the phylum level. (c) Gene abundance (log_{10} transformed) involved in N/C/S cycling reactions. CK, L, and H denote control (no eradication, 0 kg m^{-2}), low-intensity eradication (2 kg m^{-2}), and high-intensity eradication (4 kg m^{-2}), respectively.

3.5. *Environmental drivers of NO_3^- reduction pathways and N_2O emission*

To clarify the associations among environmental variables, microbial communities, and NO_3^- reduction processes, correlation and multivariate analyses were conducted (Fig. 7).

The Mantel test showed that functional microbial groups differed in their correlation patterns with environmental factors. N_2O-reducing communities (genus level) were significantly correlated with most measured variables (Fig. 7a; $p < 0.05$). NO_3^--reducing communities were mainly related to pH, TOC, C/N, and WC ($p < 0.01$). Sulfate-reducing communities were significantly correlated with various carbon, nitrogen, and sulfur-related factors ($p < 0.05$). Spearman correlation analysis further indicated that N_2O emission rates were significantly positively correlated with DNF, TN, and NO_3^- ($p < 0.01$). DNF rates were also significantly positively correlated with TN and NO_3^- ($p < 0.05$), but significantly negatively correlated with TOC: NO_3^- ($p < 0.05$). DNRA rates were significantly positively correlated with carbon and sulfur-related indicators as well as the carbon–nitrogen ratio (DOC: NO_3^-, TOC: NO_3^-) ($p < 0.01$).

RDA based on the combined phylum-level community and functional gene matrix showed that the first two axes explained 80.50% of the total constrained variance (Fig. 7b; Axis 1: 57.07%; Axis 2: 23.43%). Among the measured variables, pH, WDOC, WC, DIN, and TOC were significantly associated with variation in the combined microbial community and functional gene composition. In the sorting diagram, DNF rates were positioned in proximity to *Proteobacteria*; DNRA rates were closely associated with sulfur-reducing bacteria, carbon-degrading functional genes, *Bacillota, Bacteroidota*, and *Thermodesulfobacteria*.

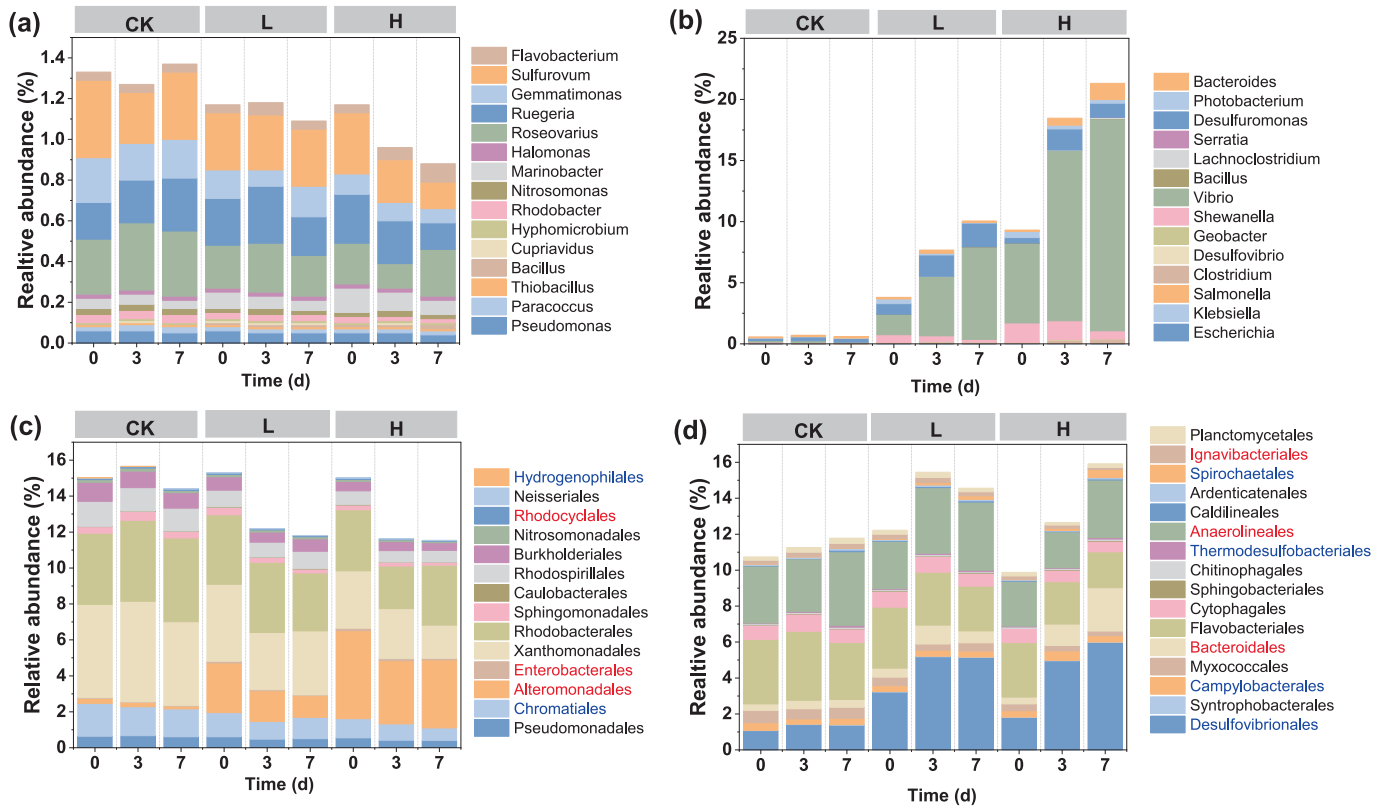


Fig. 6. The relative abundances of DNF (a), DNRA (b) microorganisms at the genus level; *nosZ-I* (c) and *nosZ-II* (d) microorganisms at the order level. Note: In figures (c) and (d), DNRA and SRB-related microorganisms are labeled in red and blue font, respectively. CK, L, and H denote control (no eradication, 0 kg m^{-2}), low-intensity eradication (2 kg m^{-2}), and high-intensity eradication (4 kg m^{-2}), respectively.

Linear regression further demonstrated that DNRA% increased significantly with increasing sediment carbon-to-nitrogen indicators (TOC: TN, TOC: NO_3^-, DOC: NO_3^-), demonstrating that increasing carbon-to-nitrate ratios were associated with a higher proportional contribution of DNRA to total NO_3^- reduction.

4. Discussions

4.1. Biogenic carbon input from S. alterniflora residues alters NO_3^- removal pathways

The input of biogenic carbon from *S. alterniflora* residues initially stimulated DNF and denitrifier proliferation. In incubation experiments, DNF accounted for 92.28% and 86.47% of NO_3^- reduction in the low and high addition, respectively—significantly higher than in the control (Fig. 4c). NO_3^- acts as a terminal electron acceptor for organic matter oxidation under anoxic conditions, facilitating DNF (Beaulieu et al., 2011; Yan et al., 2023). A strong positive correlation was observed between DNF rates and sediment NO_3^- concentrations ($p < 0.01$). RDA revealed that the abundance of *Proteobacteria*, a phylum known for its high denitrifier content (Scott et al., 2008; Yang et al., 2021), was significantly correlated with NO_3^-, DIN, and DNF rates (Fig. 7b; $p < 0.05$). This suggests that the increase in denitrifying microorganisms, particularly *Proteobacteria*, is strongly associated with the NO_3^- reduction under the addition of *S. alterniflora* residues at day 0. Consistently, the abundance of the DNF gene *nirS* increased by 29.42% and 66.67% in the low and high addition, respectively, indicating enhanced denitrifier activity and potential (Surey et al., 2020).

Intensified DNF led to rapid NO_3^- depletion in sediments under *S. alterniflora* residues input, which promoted DNRA in the later stage. Field monitoring showed that sediment NO_3^- concentrations declined by 75.58% six months after *S. alterniflora* eradication (Table 1), and NO_3^- levels fell below 1 mg kg^{-1} with plant residues additions, reflecting heightened nitrogen-limited conditions in the coastal wetland (Lovelock et al., 2006). Although DOC accumulated markedly (2–5 times higher than the control in low and high addition), it did not correlate significantly with DNF ($p > 0.05$), suggesting that DNF was primarily limited by NO_3^- concentration (Dai et al., 2024; Lovelock et al., 2006). The DNF contribution decreased from 90.26% at six months to 56.61% after two years, while the contribution of DNRA rose to 28.26–34.34%, exceeding values reported in other coastal wetlands (Table S4).

The partitioning of NO_3^- reduction was strongly regulated by carbon–nitrogen stoichiometry. The sediments TOC: NO_3^- ratio increased by 1.84 and 2.35 times after six months and one year of eradication (Table 1), respectively, with consistent trends in incubation treatments (Fig. 3h). The most significant predictor of DNRA% was the ratio of dissolved organic carbon to nitrate (DOC: NO_3^-) (Fig. 7c), which strongly supports the view that the immediate availability of labile carbon was the primary driver for the dominance of DNRA over DNF under NO_3^- limited conditions. The microbial preference for DNRA in such conditions is energetically favorable: reducing NO_3^- to NH_4^+ via DNRA consumes eight electrons but generates more energy than the five-electron DNF pathway to N_2, offering a higher energy return when carbon is abundant (Liao et al., 2025; Schmidt et al., 2011).

Moreover, taxa involved in complex carbon degradation (e.g., *Bacteroidota, Chloroflexi*) showed a significant enrichment from day 3 to day 7, along with increased abundances of functional genes associated with the breakdown of starch (*amyA/B*) and cellulose (*celB, xynA/B*) (Fig. 5b & d). These metabolic pathways likely supplied low-molecular-weight organic acids that supported both DNRA and sulfate reduction (Bonaglia et al., 2016; Wang et al., 2023c). Strong correlations between *nrfA*, *dsrB*, and DNRA rates, along with tighter network co-occurrences between sulfate-reducing bacteria and DNRA taxa (Fig. 7b & Fig. S3), indicate a coupled metabolic interplay that ultimately promoted

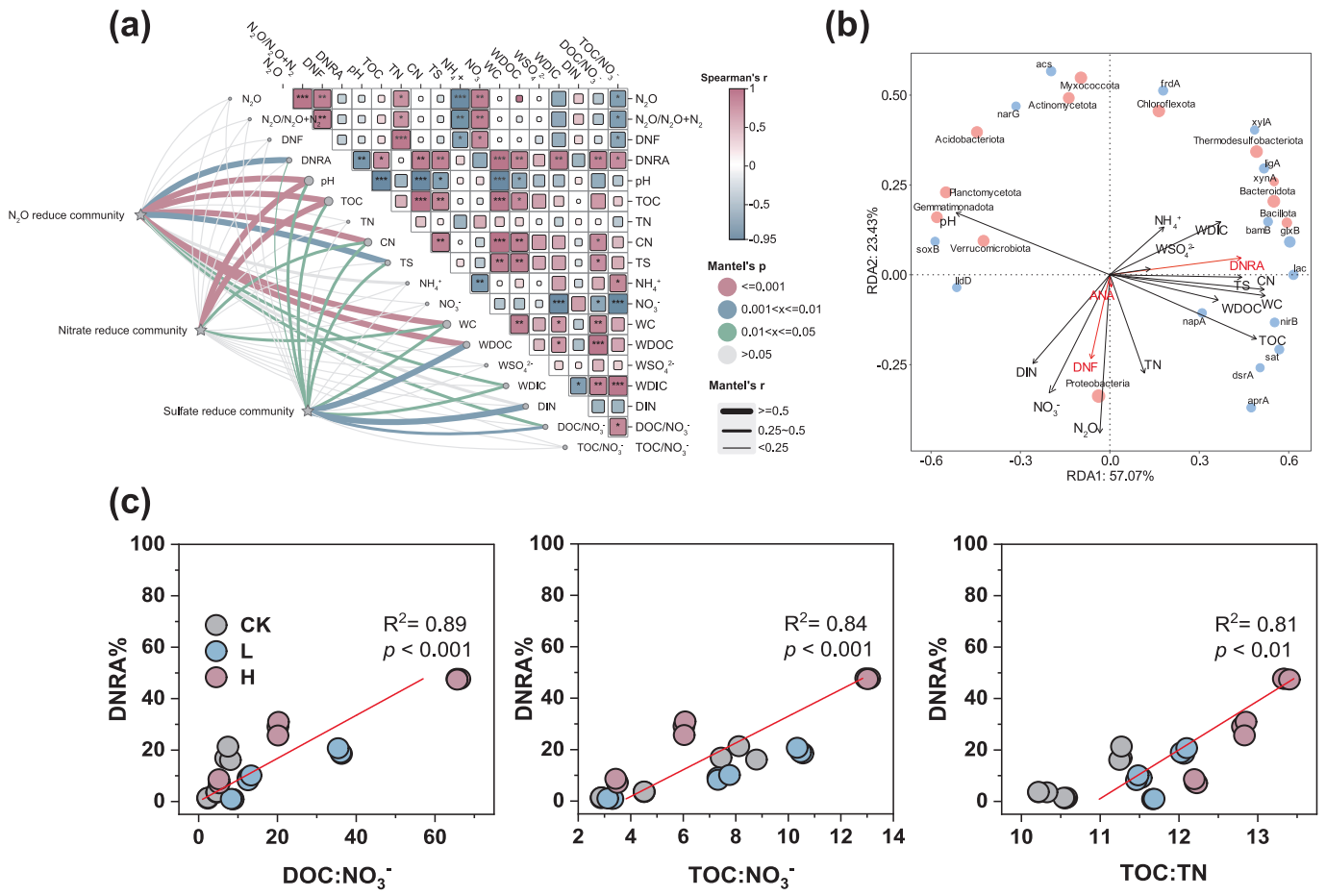


Fig. 7. Associations among environmental factors, microbial communities, and nitrogen transformation processes. (a) Mantel tests (genus level) and Spearman correlations showing relationships between environmental variables (soil physicochemical properties and overlying water parameters), functional microbial guilds (N_2O-, NO_3^--, and sulfate-reducing communities), and nitrogen transformation rates (N_2O emission, DNF, DNRA). Line colors and widths represent Mantel's r values and significance levels; square colors indicate Spearman's r. (b) Redundancy analysis (RDA) ordination illustrating the relationships among phylum-level microbial composition, functional gene profiles, environmental variables, and nitrogen transformation rates. Arrow lengths indicate the relative contribution of environmental variables to community variation. (c) Linear regressions between DNRA% and sediment carbon-to-nitrate stoichiometric ratios (DOC: NO_3^-, TOC: NO_3^-, TOC: TN) under different *S. alterniflora* residue treatments.

ammonium retention in the system (Caffrey et al., 2018; Fan et al., 2024). As a result, NH_4^+ accumulated in sediments, providing a retained nitrogen pool for the coastal ecosystem (Liao et al., 2025).

Although ANA represents an alternative N_2-producing pathway that could theoretically consume DNRA-derived NH_4^+, its contribution in this system was quantitatively minor (Fig. S4). Measured ANA rates remained low and showed no significant response to residue addition or OC enrichment (Fig. 7b). Across treatments, ANA accounted for only 6.28–15.62% of total NO_3^- reduction (Fig. 4c), consistent with previous measurements in estuarine and tidal wetlands (Table S4). These results indicate that ANA did not drive the observed re-partitioning of NO_3^- reduction.

Notably, previous studies on *S. alterniflora* invasion of mudflats have predominantly reported enhanced DNF and increased NO_3^- loss under invasion-driven carbon enrichment. These findings largely reflect conditions during active *S. alterniflora* expansion, when continuous root exudation and fresh organic matter inputs stimulate denitrifier activity (Gao et al., 2019). In contrast, the post-eradication deposits substantial amounts of plant residues into the sediments, which represent a distinct biogeochemical regime, characterized by high C/N inputs, rapid NO_3^- depletion, and intensified sulfate reduction. Under these conditions, microbial competition favored DNRA over DNF (Liao et al., 2025; Sun et al., 2021; Wei et al., 2022).

Collectively, our results indicate that *S. alterniflora* residue inputs redirected NO_3^- reduction from DNF toward DNRA, thereby increasing NH_4^+ retention in sediments. Nevertheless, retained NH_4^+ is not necessarily permanently immobilized, and its long-term fate likely depends on environmental conditions such as oxygen availability, biological uptake, and tidal exchange (Alongi et al., 2005). In our system, persistently low redox potentials combined with elevated organic carbon inputs promoted anaerobic decomposition and fermentation, which depleted oxygen and thereby constrained nitrification. Moreover, given the high clay content and strong cation exchange capacity of coastal wetland sediments, NH_4^+ is likely to be effectively retained through adsorption and particle association (Caffrey et al., 2018), further prolonging its residence time and limiting rapid export or re-oxidation. These findings underscore that *S. alterniflora* eradication modifies nitrogen cycling by altering nitrogen retention–loss dynamics, setting the stage for evaluating how this shift influences N_2O production and mitigation.

4.2. *The pathways of NO_3^- removal control N_2O emission*

The initial pulse of N_2O emission was primarily attributed to incomplete DNF, a process in which NO_3^- is reduced to N_2O instead of N_2, consistent with previous studies (Gao et al., 2019). A significant positive correlation ($p < 0.01$) between N_2O production and DNF rates was observed, which supports the idea that incomplete DNF under conditions of high NO_3^- availability can lead to increased N_2O emissions

(Fig. 7a). Field measurements recorded a post-eradication emission peak of 2.53 times than the pre-eradication annual average (12.48 μg m^{-2} h^{-1}; Fig. 2), greatly exceeding levels in natural salt marshes (Table S3). This trend was amplified in laboratory incubations, where N_2O production increased by 53 to 186-fold in the residue-amended treatments. The efficiency of biological N_2O reduction strongly regulates the release of N_2O during nitrogen cycling (Li et al., 2009), with *nosZ* activity serving as a key control (Xiang et al., 2023). *NosZ* enzyme activity is highly sensitive to pH (Su et al., 2021). Field observations recorded a decline in sediment pH from 7.70 to 7.17 six months post-treatment (Table 1), and under laboratory conditions, the low and high additions exhibited pH reductions of 0.10 and 0.24 units, respectively, compared to the control. This decline in pH reduced the abundance of *nosZ* genes by 13.6% and 23.0% in the low and high addition during the initial phase (Fig. 5c), leading to impaired N_2O reduction and an increased $N_2O/(N_2O + N_2)$ ratio. Such pH-dependent suppression of N_2O reductase activity has been documented in other estuarine sediments, which is attributed to compromised electron transfer (Frostegard et al., 2022) and enzyme function (Su et al., 2021).

The subsequent enhancement of DNRA activity contributed to the reduced N_2O emissions. DNRA, which reduces NO_3^- to NH_4^+ rather than N_2O, competes with DNF for NO_3^- and may therefore limit N_2O production (Yuan et al., 2022). Mantel analysis revealed a significant negative correlation ($p < 0.001$) between DNRA rate and N_2O emissions, further suggesting that increased DNRA activity is associated with reduced N_2O production (Fig. 7a). Under hypoxic or anaerobic conditions, NH_4^+ does not directly generate N_2O (Quick et al., 2019), and elevated NH_4^+ can further restrict NO_3^- availability by promoting its assimilation by plants or microorganisms (Liu et al., 2024). In parallel, anaerobic fermentation of *S. alterniflora* residues led to the depletion of labile organic acids, allowing sediment pH to rebound ($\Delta pH = +0.14$ in the H treatment; Fig. S2a). This pH recovery alleviated acid-mediated inhibition of *nosZ*, and the relative abundance of *nosZ* genes in low and high addition increased by 14.1% and 51.5%, respectively (Fig. 5), coinciding with a significant decrease in $N_2O/(N_2O + N_2)$ ratios, indicating enhanced N_2O reduction.

Additionally, *S. alterniflora* residue additions significantly increased the abundance of bacterial taxa associated with DNRA and sulfate reduction, including *Bacteroidota, Thermodesulfobacteriota, and Bacillota* (Fig. 5b). These phyla are known to harbor *nosZ-II*–carrying microorganisms, which are crucial for efficient N_2O reduction in anoxic or sulfidic conditions (Chutivisut et al., 2018; Fan et al., 2024). At the order level, community composition revealed enrichment of sulfate-reducing groups such as *Desulfovibrionales, Campylobacterales, and Spirochaetales*, as well as DNRA-associated taxa including *Alteromonadales, Bacteroidales, and Anaerolineales* in low and high addition (Fig. 6b). Notably, *nosZ-II* enzymes from taxa such as *Desulfovibrionales and Bacteroidales* exhibit sulfide tolerance and preferential expression under reduced, sulfidic conditions (Nie et al., 2021; Sanford et al., 2012). Together, these data indicate that the proliferation of *nosZ*-II–dominant microbial communities with enhanced N_2O-reducing capabilities likely contributed to the observed decline in N_2O emissions. The enrichment of sulfide-tolerant *nosZ-II* taxa indicates that SRB-driven environments can promote complete N_2O reduction, suggesting that managing sediment redox states is key to minimizing greenhouse gas emissions during restoration. Besides DNRA competition and *nosZ*-mediated N_2O reduction, ANA provides an N_2-forming pathway that does not produce N_2O (Song et al., 2013), but its contribution in our system was minor (Fig. 4c).

Collectively, while early DNF pulses temporarily enhanced NO_3^- removal, the subsequent shift toward DNRA retained nitrogen as NH_4^+ in sediments, reducing net nitrogen loss.. This reveals a critical ecosystem trade-off: *S. alterniflora* eradication transforms the wetland from a potent source of the greenhouse gas N_2O into a sink, yet nitrogen remains temporarily bioavailable rather than permanently removed. Future work should integrate tidal dynamics and redox heterogeneity to predict ecosystem-scale outcomes.

5. Conclusion

This study demonstrates that the eradication of *S. alterniflora* induces a marked shift in NO_3^- removal pathways, primarily driven by plant residue-mediated changes in carbon substrate availability and microbial community. In the early stage, sufficient NO_3^- and denitrifying bacteria stimulated DNF but also caused incomplete DNF, leading to transient N_2O pulses. Subsequently, the system shifted toward a higher proportion of DNRA, facilitated by elevated C/NO_3^- ratios and reduced NO_3^- availability. The enrichment of fermentative and sulfate-reducing taxa, together with increased *nrfA* and the *nosZ*-II-type N_2O-reducing microbes, supported this transition and mitigated N_2O emission. While DNRA enhances nitrogen retention as NH_4^+, it may also increase the risk of NH_4^+ export to estuaries. By unraveling the mechanistic linkages between *S. alterniflora* eradication, NO_3^- removal pathway shifts, and the transition of N_2O emissions from source to sink, this work provides a critical theoretical foundation for achieving coordinated nutrient removal and climate mitigation benefits in coastal wetland restoration.

CRediT authorship contribution statement

Shiyao Chen: Writing – review & editing, Writing – original draft, Methodology, Investigation, Formal analysis, Data curation, Conceptualization. **Hui Wu:** Writing – review & editing, Investigation, Data curation. **Wenhong Xu:** Investigation, Data curation. **Fenfang Wang:** Writing – review & editing. **Ruifeng Yan:** Writing – review & editing. **Shaobin Li:** Writing – review & editing. **Nengwang Chen:** Writing – review & editing, Supervision, Resources, Project administration, Funding acquisition, Conceptualization.

Declaration of competing interest

The authors declare that they have no known competing financial interests or personal relationships that could have appeared to influence the work reported in this paper.

Acknowledgements

This research was supported by the National Natural Science Foundation of China (No. 42276171), the National Key R&D Program of China (2022YFF0802102), and the Shenzhen Science and Technology Plan Project (KCXST20221021111404011). We are grateful to Wenyan Tang, Chunyan Cheng, Mengru Li, and Yuyang Zheng for their assistance with field measurements, and to Junhui Chen, Fang Wu, Junou Du, and Lei Wang for their supportive technical work. We also thank Yihui Zhang and Yasong Chen for their data supporting *S. alterniflora* biomass.

Appendix A. Supplementary data

Supplementary data to this article can be found online at https://doi.org/10.1016/j.geoderma.2026.117780.

Data availability

Data will be made available on request.

References

Aelion, C.M., Warttinger, U., 2010. Sulfide inhibition of nitrate removal in coastal sediments. Estuaries 33 (3), 798–803.

Alongi, D.M., Clough, B.F., Robertson, A.I., 2005. Nutrient-use efficiency in arid-zone forests of the mangroves Rhizophora stylosa and Avicennia marina. Aquat. Bot. 82 (2), 121–131.

Beaulieu, J.J., Tank, J.L., Hamilton, S.K., Wollheim, W.M., Hall, R.O., Mulholland, P.J., Peterson, B.J., Ashkenas, L.R., Cooper, L.W., Dahm, C.N., Dodds, W.K., Grimm, N.B.,

Johnson, S.L., McDowell, W.H., Poole, G.C., Valett, H.M., Arango, C.P., Bernot, M.J., Burgin, A.J., Crenshaw, C.L., Helton, A.M., Johnson, L.T., O'Brien, J.M., Potter, J.D., Sheibley, R.W., Sobota, D.J., Thomas, S.M., 2011. Nitrous oxide emission from denitrification in stream and river networks. PNAS 108 (1), 214–219.
Bonaglia, S., Klawonn, I., De Brabandere, L., Deutsch, B., Thamdrup, B., Brüchert, V., 2016. Denitrification and DNRA at the Baltic Sea oxic-anoxic interface: Substrate spectrum and kinetics. Limnol. Oceanogr. 61 (5), 1900–1915.
Buchfink, B., Xie, C., Huson, D.H., 2015. Fast and sensitive protein alignment using diamond. Nat. Meth. 12 (3), 59–60.
Burgin, A.J., Hamilton, S.K., 2007. Have we overemphasized the role of denitrification in aquatic ecosystems? A review of nitrate removal pathways. Front. Ecol. Environ. 5 (2), 89–96.
Caffrey, J.M., Bonaglia, S., Conley, D.J., 2018. Short exposure to oxygen and sulfide alter nitrification, denitrification, and DNRA activity in seasonally hypoxic estuarine sediments. FEMS Microbiol. Lett. 366 (1), fny288.
Chen, C., Yin, G., Li, Q., Gu, Y., Sun, D., An, S., Liang, X., Li, X., Zheng, Y., Hou, L., Liu, M., 2023. Effects of microplastics on denitrification and associated N_2O emission in estuarine and coastal sediments: insights from interactions between sulfate reducers and denitrifiers. Water Res. 245, 120590.
Chen, N., Wu, J., Duan, H., Wei, T., 2010. N2: Ar method for direct measurement of denitrification product (dissolved N2) using membrane inlet mass spectrometry (MIMS). Acta Sci. Circumstantiae 30 (12), 2479–2483.
Chen, S., Gao, D., Zhang, J., Müller, C., Li, X., Zheng, Y., Dong, H., Yin, G., Han, P., Liang, X., Liu, M., Hou, L., 2022. Invasive Spartina alterniflora accelerates soil gross nitrogen transformations to optimize its nitrogen acquisition in an estuarine and coastal wetland of China. Soil Biol. Biochem. 174, 108835.
Chiu, C.-Y., Lee, S.-C., Chen, T.-H., Tian, G., 2004. Denitrification associated N loss in mangrove soil. Nutr. Cycl. Agroecosyst. 69, 185–189.
Chutivisut, P., Isobe, K., Powtongsook, S., Pungrasmi, W., Kurisu, F., 2018. Distinct microbial community performing dissimilatory nitrate reduction to ammonium (DNRA) in a high C/NO_3^- reactor. Microbes Environ. 33 (3), 264–271.
Crow, S.E., Lajtha, K., Bowden, R.D., Yano, Y., Brant, J.B., Caldwell, B.A., Sulzman, E.W., 2009. Increased coniferous needle inputs accelerate decomposition of soil carbon in an old-growth forest. For. Ecol. Manag. 258 (10), 2224–2232.
Dai, Z., Zhang, N., Ma, X., Wang, F., Peng, J., Yang, S., Cao, W., 2024. Microplastics strengthen nitrogen retention by intensifying nitrogen limitation in mangrove ecosystem sediments. Environ. Int. 185, 108546.
Fan, Y., Zhou, Z., Liu, F., Qian, L., Yu, X., Huang, F., Hu, R., Su, H., Gu, H., Yan, Q., He, Z., Wang, C., 2024. The vertical partitioning between denitrification and dissimilatory nitrate reduction to ammonium of coastal mangrove sediment microbiomes. Water Res. 262, 122113.
Fazzolari, É., Nicolardot, B., Germon, J.C., 1998. Simultaneous effects of increasing levels of glucose and oxygen partial pressures on denitrification and dissimilatory nitrate reduction to ammonium in repacked soil cores. Eur. J. Soil Biol. 34, 47–52.
Feng, Y., Jiang, W., Liu, Y., 2024. Effects of plowing and plant residue mulching on soil nitrous oxide emissions in a black soil beachtype degraded grassland. Acta Prataculturae Sin. 33 (11), 15–29.
Frostegard, A., Vick, S.H.W., Lim, N.Y.N., Bakken, L.R., Shapleigh, J.P., 2022. Linking meta-omics to the kinetics of denitrification intermediates reveals pH-dependent causes of N_2O emissions and nitrite accumulation in soil. ISME J. 16 (1), 26–37.
Gao, G., Li, P., Zhong, J., Shen, Z., Chen, J., Li, Y., Isabwe, A., Zhu, X., Ding, Q., Zhang, S., Gao, C., Zheng, H., 2019. Spartina alterniflora invasion alters soil bacterial communities and enhances soil N_2O emissions by stimulating soil denitrification in mangrove wetland. Sci. Total Environ. 653, 231–240.
Hou, L., Yin, G., Liu, M., Zhou, J., Zheng, Y., Gao, J., Zong, H., Yang, Y., Gao, L., Tong, C., 2014. Effects of sulfamethazine on denitrification and the associated N_2O release in estuarine and coastal sediments. Environ. Sci. Technol. 49 (1), 326–333.
Huang, M., Zhang, Y. and Zhou, Z., 2023. A dataset of the UAV remote sensing spatial distribution of Spartina alterniflora in the Zhangjiang Estuary of Fujian Province from 2013 to 2022. Science Data Bank.
Hyatt, D., Chen, G.-L., LoCascio, P.F., L, M.L., Larimer, F.W. and Hauser, L.J., 2010. Prodigal: prokaryotic gene recognition and translation initiation site identification. BMC Bioinf. 11(1), 119.
IPCC, 2021 Contribution of working group i to the sixth assessment report of the intergovernmental panel on climate change, Cambridge University.
Jia, D., Qi, F., Xu, X., Feng, J., Wu, H., Guo, J., Lu, W., Peng, R., Zhu, X., Luo, Y., Lin, G., 2016. Co-regulations of Spartina alterniflora invasion and exogenous nitrogen loading on Soil N_2O efflux in subtropical mangrove mesocosms. PLoS One 11 (1), e0146199.
Kuzyakova, Y., Friedelb, J.K., Stahra, K., 2000. Review of mechanisms and quantification of priming effects. Soil Biol. Biochem. 32, 1485–1498.
Lee, C., Kim, D.U., Lee, J., Kwon, I., Kim, Y.E., Yi, G., Kim, T., Yoon, S.J., Kim, J.J., Khim, J.S., 2026. Effects of litter decomposition on sedimentary organic carbon sequestration in invasive and native halophyte marshes of Ganghwa, Korea. Mar. Pollut. Bull. 222 (Pt 2), 118727.
Li, R., Yu, C., Li, Y., Lam, T.-W., Yiu, S.-M., Kristiansen, K., Wang, J., 2009. SOAP2: an improved ultrafast tool for short read alignment. Bioinformatics 25 (15), 1966–1967.
Liao, Y., He, T., Wang, C., Zheng, C., Zhang, M., 2025. Dissimilatory nitrate reduction to ammonium has a competitive advantage over denitrification under nitrate-limited conditions. Rev. Environ. Sci. Biol. 24, 97–114.
Liu, C., Ma, J., Wang, M., Xu, J., Zhu, C., Zhu, G., 2024. Electrocatalytic nitrate reduction using iron single atoms for sustainable ammonium supplies to increase rice yield. PNAS 121 (50), e2408187121.
Lopez-Ponnada, E.V., Lynn, T.J., Peterson, M., Ergas, S.J., Mihelcic, J.R., 2017. Application of denitrifying wood chip bioreactors for management of residential non-point sources of nitrogen. J. Biol. Eng. 11 (1), 16.
Lovelock, C.E., Feller, I.C., Ball, M.C., Engelbrecht, B.M.J., Ewe, M.L., 2006. Differences in plant function in phosphorus- and nitrogen-limited mangrove ecosystems. New Phytol. 172 (3), 514–522.
Lu, Z., Xiao, K., Wang, F., Wang, Y., Yu, Q., Chen, N., 2023. Salt marsh invasion reduces recalcitrant organic carbon pool while increases lateral export of dissolved inorganic carbon in a subtropical mangrove wetland. Geoderma 437, 116573.
Martin, M., 2011. Cutadapt removes adapter sequences from high-throughput sequencing reads. Embnet J 17, 10–12.
McCall, B.D., Pennings, S.C., 2012. Geographic variation in salt marsh structure and function. Oecologia 170 (3), 777–787.
Nie, S., Zhang, Z., Mo, S., Li, J., He, S., Kashif, M., Liang, Z., Shen, P., Yan, B., Jiang, C., 2021. Desulfobacterales stimulates nitrate reduction in the mangrove ecosystem of a subtropical gulf. Sci. Total Environ. 769, 144562.
O'Nuanain, A., Benelli, A., Winston, J., Swenson, E.M., López-Duarte, P.C., Roberts, B.J., Polito, M.J., 2025. Decomposition of Spartina alterniflora (smooth cordgrass) in coastal Louisiana brackish marshes influenced by a freshwater siphon. Discov. Ecol 1 (1), 16.
Quick, A.M., Reeder, W.J., Farrell, T.B., Tonina, D., Feris, K.P., Benner, S.G., 2019. Nitrous oxide from streams and rivers: a review of primary biogeochemical pathways and environmental variables. Earth Sci. Rev. 191, 224–262.
Sanford, R.A., Wagner, D.D., Wu, Q., Chee-Sanford, J.C., Thomas, S.H., Cruz-García, C., Rodríguez, G., Massol-Deyá, A., Krishnani, K.K., Ritalahti, K.M., Nissen, S., Konstantinidis, K.T., Löffler, F.E., 2012. Unexpected nondenitrifier nitrous oxide reductase gene diversity and abundance in soils. Proc. Natl. Acad. Sci. 109 (48), 19709–19714.
Schmidt, C.S., Richardson, D.J., Baggs, E.M., 2011. Constraining the conditions conducive to dissimilatory nitrate reduction to ammonium in temperate arable soils. Soil Biol. Biochem. 43 (7), 1607–1611.
Scott, J.T., McCarthy, M.J., Gardner, W.S., Doyle, R.D., 2008. Denitrification, dissimilatory nitrate reduction to ammonium, and nitrogen fixation along a nitrate concentration gradient in a created freshwater wetland. Biogeochemistry 87 (1), 99–111.
Shao, B., Xie, Y.-G., Zhang, L., Ruan, Y., Liang, B., Zhang, R., Xu, X., Wang, W., Lin, Z., Pei, X., Wang, X., Zhao, L., Zhou, X., Wu, X., Xing, D., Wang, A., Lee, D.-J., Ren, N., Canfield, D.E., Hedlund, B.P., Hua, Z.-S., Chen, C., 2025. Versatile nitrate-respiring heterotrophs are previously concealed contributors to sulfur cycle. Nat. Commun. 16 (1), 1202.
Song, G.D., Liu, S.M., Marchant, H., Kuypers, M.M.M., Lavik, G., 2013. Anammox, denitrification and dissimilatory nitrate reduction to ammonium in the East China Sea sediment. BG 10 (11), 6851–6864.
Song, N., He, Y.-H., Jiang, H.-L., 2016. Inferior adaptation of bay sediments in a eutrophic shallow lake to winter season for organic matter decomposition. Environ. Pollut. 219, 794–803.
Steinegger, M., Söding, J., 2017. MMseqs2 enables sensitive protein sequence searching for the analysis of massive data sets. Nat. Biotechnol. 35 (11), 1026–1028.
Stokstad, E., 2023. China battles alien weed at unprecedented scale. Sccience 379 (6636), 972.
Su, X., Wen, T., Wang, Y., Xu, J., Cui, L., Zhang, J., Xue, X., Ding, K., Tang, Y., Zhu, Y.G., 2021. Stimulation of N_2O emission via bacterial denitrification driven by acidification in estuarine sediments. Glob. Chang. Biol. 27 (21), 5564–5579.
Sun, F., Deng, Q., Li, X., Tang, M., Ma, X., Cao, X., Zhou, Y., Song, C., 2021. Organic carbon quantity and quality jointly triggered the switch between dissimilatory nitrate reduction to ammonium (DNRA) and denitrification in biofilters. Chemosphere 280, 130917.
Surey, R., Schimpf, C.M., Sauheitl, L., Mueller, C.W., Rummel, P.S., Dittert, K., Kaiser, K., Böttcher, J., Mikutta, R., 2020. Potential denitrification stimulated by water-soluble organic carbon from plant residues during initial decomposition. Soil Biol. Biochem. 147, 107841.
Tang, L., Zhou, Q.S., Guo, W., Li, P., Gao, Y., 2021. Importance of high severity in a physical removal treatment for controlling invasive Spartina alterniflora. Ecol. Eng. 171, 106375.
Tao, J., Xu, H., Zhang, T., You, Z., Shah, K.J., 2022. Study on reed straw carbon source-enhanced nitrogen removal effect in wetland system. Water Air Soil Pollut. 233 (11), 429.
Wang, B., Lin, X., 2023. Exotic Spartina alterniflora invasion enhances sediment N-loss while reducing N retention in mangrove wetland. Geoderma 431, 116362.
Wang, F., Lu, Z., Tobias, C.R., Wang, Y., Xiao, K., Yu, Q., Lin, J., Huang, G., Chen, N., 2023a. Salt marsh expansion into estuarine mangrove mudflats reduces nitrogen removal capacity. Catena 232, 107459.
Wang, F., Song, A., Zhang, Y., Lin, X., Yan, R., Wang, Y., Chen, N., 2022. Saltmarsh sediments with wastewater input emit more carbon greenhouse gases but less N_2O than mangrove sediments. Catena 213, 106205.
Wang, J., Sun, Z., He, T., Gao, H., Wang, H., Li, X., 2019a. Effects of siltation by Spartina alterniflora invasion on decomposition of and sulfur release by S. alterniflora and Cyperus malaccensis in tidal marshes of the MIn River Estuary. Acta Ecol. Sin. 39 (10), 3631–3642.
Wang, K., Wang, S., Zhang, X., Wang, W., Li, F., Dong, L., Kong, F., Xi, M., 2023b. Potential ecological impacts of physical control on Spartina alterniflora in coastal wetland: Migration and transformation of nutrients and the response of bacterial community structure. J. Clean. Prod. 398, 136556.
Wang, L., Han, X., Zhang, Y., Zhang, Q., Wan, X., Liang, T., Song, H., Bolan, N., Shaheen, S.M., White, J.R., Rinklebe, J., 2023c. Impacts of land uses on spatio-temporal variations of seasonal water quality in a regulated river basin, Huai River, China. Sci. Total Environ. 857 (Pt 2), 159584.
Wang, W., Yang, M., Shen, P., Zhang, R., Qin, X., Han, J., Li, Y., Wen, X., Liao, Y., 2019c. Conservation tillage reduces nitrous oxide emissions by regulating functional genes

for ammonia oxidation and denitrification in a winter wheat ecosystem. Soil Tillage Res. 194, 104347.
Wei, Z., Senbayram, M., Zhao, X., Li, C., Jin, K., Wu, M., Rahman, M.M., Shan, J., Yan, X., 2022. Biochar amendment alters the partitioning of nitrate reduction by significantly enhancing DNRA in a paddy field. Biochar 4 (1), 44.
Wen, T., Xie, P., Yang, S., Niu, G., Liu, X., Ding, Z., Xue, C., Liu, Y.X., Shen, Q., Yuan, J., 2022. ggClusterNet: an R package for microbiome network analysis and modularity-based multiple network layouts. iMeta 1 (3), e32.
Xiang, H., Hong, Y., Wu, J., Wang, Y., Ye, F., Hu, Z., Qu, Z., Long, A., 2023. NosZ-II-type N_2O-reducing bacteria play dominant roles in determining the release potential of N_2O from sediments in the Pearl River Estuary, China. Environ. Pollut. 329, 121732.
Xu, J., Huang, X., Luo, P., Zhang, M., Liu, F., Xiao, R., Wu, J., 2023. Effect of plant-self debris on nitrogen removal, transformation and microbial community in mesocosm constructed wetlands planted with Myriophyllum aquaticum. J. Environ. Manag. 340, 117981.
Yan, R., Wang, F., Wang, Y., Chen, N., 2023. Pollution abatement reducing the river N_2O emissions although it is partially offset by a warming climate: Insights from an urbanized watershed study. Water Res. 236, 119934.
Yang, Z., Zhou, Q., Sun, H., Jia, L., Zhao, L., Wu, W., 2021. Metagenomic analyses of microbial structure and metabolic pathway in solid-phase denitrification systems for advanced nitrogen removal of wastewater treatment plant effluent: a pilot-scale study. Water Res. 196, 117067.
Yuan, D., Wang, G., Hu, C., Zhou, S., Clough, T.J., Wrage-Mönnig, N., Luo, J., Qin, S., 2022. Electron shuttle potential of biochar promotes dissimilatory nitrate reduction to ammonium in paddy soil. Soil Biol. Biochem. 172, 108760.
Yuan, J., Ding, W., Liu, D., Kang, H., Freeman, C., Xiang, J., Lin, Y., 2015. Exotic Spartina alterniflora invasion alters ecosystem-atmosphere exchange of CH_4 and N_2O and carbon sequestration in a coastal salt marsh in China. Glob. Chang. Biol. 21 (4), 1567–1580.
Zheng, Y., Hou, L., Liu, M., Liu, Z., Li, X., Lin, X., Yin, G., Gao, J., Yu, C., Wang, R., Jiang, X., 2016. Tidal pumping facilitates dissimilatory nitrate reduction in intertidal marshes. Sci. Rep. 6 (1), 21338.
Zhu, K., Ye, X., Ran, H., Zhang, P., Wang, G., 2022. Contrasting effects of straw and biochar on microscale heterogeneity of soil O_2 and pH: implication for N_2O emissions. Soil Biol. Biochem. 166, 108564.
Zhu, X., Ma, M., Li, L., Li, M., 2024. Impacts of intensive smooth cordgrass removal on net ecosystem exchange in a saltmarsh-mangrove ecotone of Southeast China. Sci. Total Environ. 934, 173202.
Zhu, X., Meng, L., Zhang, Y., Weng, Q., Morris, J., 2019. Tidal and meteorological influences on the growth of invasive Spartina alterniflora: evidence from UAV remote sensing. Remote Sens. (Basel) 11 (10), 1208.